MIXING IN SCRAPED SURFACE HEAT EXCHANGER GEOMETRY USING MRI

WEI WANG, JEFFREY H. WALTON[1] and KATHRYN L. MCCARTHY[2]

Department of Biological and Agricultural Engineering
[1]NMR Facility
University of California, Davis
Davis, CA 95616

Accepted for Publication July 19, 2000

ABSTRACT

Mixing, as a unit operation, is a key component in the operation of scraped surface heat exchangers (SSHE) because of its importance in ensuring uniform heat treatment. In this study, two approaches were used to evaluate mixing effectiveness in a process geometry that simulates a closed type SSHE: the strain distribution function which was based on velocity profiles and statistical mixing indices based on concentration profiles. For the 1% carboxymethyl cellulose test solution under laminar flow conditions, the lower angular rotation speed and lower axial flow rate promoted mixing with respect to mixing intensity. The residence time, as characterized by the axial Reynolds Number, was the key factor for this statistic. The strain distribution function and mixing length scale were affected by the relative contribution of angular rotation to axial flow, which was expressed as the ratio of the angular Reynolds number to the axial Reynolds number. This work demonstrates the equivalence of evaluating mixedness by experimental concentration profiles and theoretical velocity profiles.

INTRODUCTION

Scraped Surface Heat Exchange

Scraped surface heat exchangers (SSHE) are used extensively in the food processing industry to heat and cool highly viscous fluids. To best accomplish heating/cooling, operating conditions of the scraped surface heat exchanger must promote the mixing of fluid components. These components are the major component, which is the bulk fluid in the annulus, and the minor component, which is the layer of fluid being removed by the scraper at the heat exchange

[2] To whom correspondence should be addressed. TEL: 530-752-1487; FAX: 530-752-4759; E-mail: klmccarthy@ucdavis.edu

Journal of Food Process Engineering **23** (2000) 403-418.

surface. The two components are essentially the same material; however, they have slightly different physical properties, particularly viscosity, due to temperature differences. In the mixing process, product uniformity is a function of both the angular and axial flow of the fluid. The angular motion due to the rotor plays an important role in the goodness of mixing, whereas the axial motion due to pressure driven flow controls the residence time.

In many studies, research on scraped surface heat exchange has focused on the heat treatment in terms of heat transfer, residence time distribution and power consumption related to the operating conditions (Kool 1958; Bott *et al.* 1968; Alcairo and Zuritz 1990; Ramaswamy *et al.* 1995). Several studies have specifically evaluated the flow patterns in the scraped surface heat exchanger (Trommelen and Beek 1971; Corbett *et al.* 1995; Wang *et al.* 1999). Typically for single phase products, the rotational flow is in either the laminar or transition regime, and the axial flow is in the laminar regime. The results of these studies indicate that these flow patterns promote laminar mixing, which is mixing by imposed deformation (*e.g.*, strain).

With respect to mixing in general, fluids in process equipment have been analyzed by two different approaches: statistically from concentration profiles or in terms of the strain history derived from velocity profiles. The analysis of mixing using statistics is the more flexible approach of the two since it can be conducted on any type of mixer for fluid in either laminar, transition, or turbulent flow. A specified volume or cross sectional area of sample is examined for mixing intensity and/or mixing length scale. Mixing intensity is based on the difference between the undistributed component concentration and the mean concentration as expressed by the sample variance. Mixing length scale is a measure of the size of the undistributed component in the mixture and is determined through the correlation coefficient (Middleman 1977; Tadmor and Gogos 1979). Prior to tomographic methods (*e.g.*, image analysis), this type of measurement required a large number of samples and was extremely tedious. Although useful to describe the state of mixedness, these statistical parameters lack a specific relationship to operating conditions, mixer geometry, and fluid properties.

In contrast, the analysis of mixing using flow patterns reflects the geometry of the mixer, the operating conditions and the physical properties of the fluid (Bigg and Middleman 1974; Pinto and Tadmor 1970). For fluids in laminar flow, the strain history analysis provides weighted average total strain (WATS) as a measure of mixedness. Total strain and its integral, WATS, reflect the amount of deformation that a fluid element or volume undergoes. The strain imposed on the fluid element increases the interfacial area and decreases the striation thickness. Therefore, the mixing length scale decreases and product homogeneity improves. For certain geometries, such as single-screw extruders, theoretical velocity profiles, residence time distributions and strain history are

found extensively in the literature for Newtonian and power law fluids (Griffith 1962; McKelvey 1962; Booy 1963; Bigg and Middleman 1974; Middleman 1977; Harper 1981).

Tomographic Technique: Magnetic Resonance Imaging

Many types of tomographic techniques have been developed to resolve temporal and spatial coordinates of phase distributions and/or velocity profiles. The tomographic techniques are, by definition, noninvasive and nonintrusive methods to obtain information about systems. These methods are based on: electric, optic, acoustic, or magnetic properties of the material being evaluated. Dyakowski (1996) has reviewed the use of these techniques and their application in the food and chemical industries. Magnetic resonance imaging (MRI), as a tomographic technique, is uniquely suited to obtain both concentration and velocity profiles within process geometries.

Magnetic resonance techniques have become an integral part of studying mechanism that occur in food systems (McCarthy 1994). With respect to processing applications, Corbett *et al.* (1995) established that mixing and demixing occurs in rotating geometries that simulate Couette geometry, scraped surface heat exchangers and single screw extruders. These studies specifically identified geometries that allowed experimental flow simulations for the two limiting geometries of scraped surface heat exchangers: open type and closed type. For the open type flow, the blades allow flow-through in the annular region. This flow behavior is modeled as helical flow, which is superimposed Couette flow due to the rotating member and pressure-driven axial flow. In contrast, the closed type geometry blocks flow in the angular direction as the fluid is swept by the blade. The velocity profile in the θ-direction for closed blades is similar to pressure driven flow between parallel surfaces. In the experimental geometry of the closed type system, the blade sweeps the entire volume of the annular gap to create the maximum pressure-driven flow in the θ-direction. Similar to the open type, the axial flow in the z-direction is superimposed on the flow in the θ-direction. Wang *et al.* (1999) theoretically and experimentally established the role of angular velocity in the closed type geometry. This study continued the work in the SSHE geometry and focused on the relationship between the theoretical analysis of mixing through velocity profiles and the statistical analysis of mixing using concentration profiles.

In other research laboratories, Smith *et al.* (1995) assessed the quality of mixing during repetitive orifice flow with MRI. Repetitive orifice flow is distributive mixing. In contrast to the ordered distributive mixing, that occurs in such geometries as the static mixer, the orifice flow apparatus created a random flow pattern, typically referred to as random distributive mixing. In addition, these researchers evaluated laminar shear mixing in a Couette device.

The intent of these studies was to successfully demonstrate the ability of MRI to follow mixing effects between two liquids of differing NMR characteristics.

Although the focus of the work was not mixing, Rombach *et al.* (1998) obtained velocity profiles of Newtonian fluids in laminar flow in a Kenics static mixer. Like Wang (1997), this research advanced the use of MRI to obtain velocity fields in complex geometry.

The objective of this work was to evaluate the mixing of non-Newtonian test fluids in the closed type SSHE geometry at different axial flow rate and angular rotation. The mixing was quantified in two ways, by strain analysis via velocity profiles and statistically through MR concentration images. These mixing parameters are discussed in terms of axial and annular Reynolds Numbers and their ratio.

MATERIALS AND METHODS

For MRI experiments, the process geometry must be nonmagnetic. Therefore, the SSHE geometry was designed and fabricated in plastic materials (Fig. 1). The outer acrylic cylinder was 3.81 cm ID by 30 cm in length. To simulate the closed type SSHE, a straight 0.318 cm × 0.953 cm polyethylene-terephthalate (PET) blade that spanned the annular gap was attached to a 1.91 cm diameter PET cylinder. The inner cylinder was rotated by a motor that was located away from the magnetic field. Two test fluids were pumped to the unit, the major and the minor components. The major component was pumped into the scraped surface heat exchanger through the major component reservoir (Fig. 1). The minor component was fed into the annular region directly through one of three inlet ports on the outer cylinder. It was introduced at a pressure that was insufficient to disturb the established flow field in the SSHE. The test fluids were a 1% carboxymethyl cellulose (CMC) solution with power law indices of $K=30.75$ dyne cm^{-2} s^n and $n=0.72$. These indices were obtained using a Haake RV20, MV I sensor over a shear rate range of 0 - 10 s^{-1} (Geburder Haake GmbH, Karlsruhe, Germany). The density of the solution was 1.004 g cm^{-3}. The experimental operating conditions were inner cylinder rotation rates of 7.5 and 15 rpm and volumetric flow rates of 45 and 92 mL/min.

The MR image, obtained at the cross section designated by P-P, is a representative example of uniform hydrogen signal intensity that is typical of 100% major component (Fig. 1). As with all images in this study, it was obtained using a General Electric CSI-II/TecMag Libra spectrometer connected to a 0.6 T Oxford superconducting magnet (corresponding to 25.9 MHz for the ^1H resonance frequency). A birdcage coil was used to transmit and receive the radio frequency signal. The minor component was distinguished from the major component in the proton density images by the addition of an NMR doping

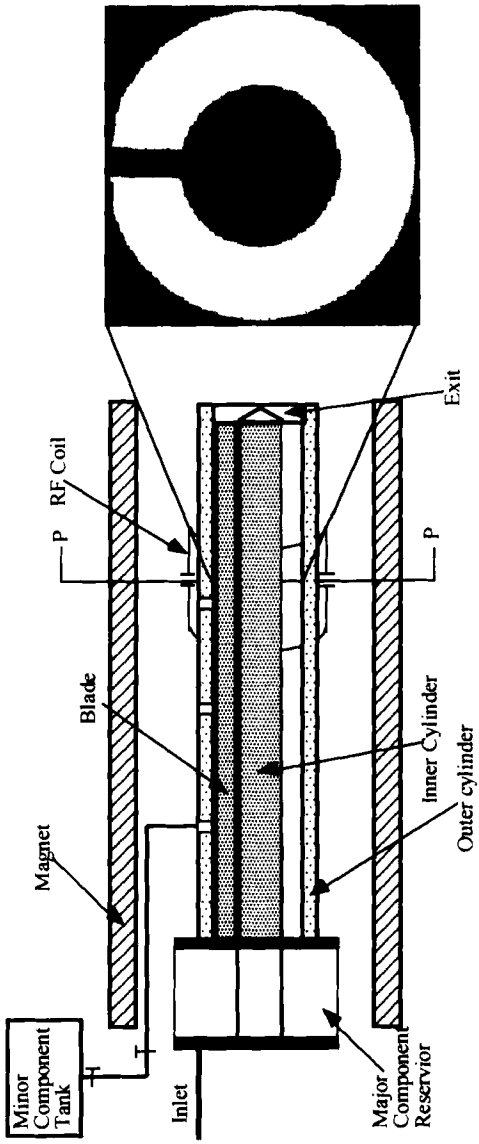

FIG. 1. SCHEMATIC OF EXPERIMENTAL SSHE APPARATUS

compound. Doping compounds alter the magnetic resonance properties of the test fluid at very low concentrations (<0.1%), without significant change to the physical properties of the fluid. In this study, manganese chloride ($MnCl_2 \cdot 4H_2O$) was added to the 1% CMC test fluid at a level of 0.068%. The doped fluid had shorter spin-lattice and spin-spin relaxation times (T_1 and T_2, respectively) which was reflected by a lower signal intensity than the undoped fluid.

The signal intensity (*SI*) is determined through its unique relationship with spin-lattice and spin-spin relaxation times of the materials, as well as the experimental conditions, the repetition time and the echo time:

$$SI = m * \left[1 - \exp\left(\frac{TR}{T_1}\right)\right] * \exp\left(-\frac{TE}{T_2}\right) \quad (1)$$

where *TR* is the repetition time, *TE* is the echo time, and *m* is a constant related to the sample and its chemical and physical environment. The proton density images were spin-echo T_2-weighted images (Wang *et al.* 1998).

Due to the exponential nature of the relationship, a calibration curve was developed for the test fluids in this study (Fig. 2). This figure illustrates the change in signal intensity as a function of the percent of doped minor component. The *x*-axis is plotted as the relative signal intensity in percent, which was normalized using the signal intensity of the pure major component. The *y*-axis plots the percent of minor component, a value of 0 means pure major component and 100% represents pure minor component. Individual pixel signal intensities in an image were then converted to the minor component concentration. In the process of converting signal intensity to the concentration, if the pixel signal intensity was less than 4.9%, the pixel was considered to contain pure minor component. At the other extreme, if the signal intensity was greater than 97%, the pixel was considered to contain pure major component only. The procedure was justified due to the lack of curve fit at high signal intensity and that most pixel intensities fell midrange.

In addition to the MR concentration profiles, velocity profiles in the apparatus also provide a means to characterize mixing under laminar flow conditions through the WATS. A fluid dynamics analysis package software, FIDAP (Fluent Inc., Evanston, IL), based on finite element analysis was used to obtain three-dimensional velocity profiles for the experimental apparatus. The mesh geometry, composed of eight-node brick elements, modeled fluid region between the 1.91 cm diameter inner cylinder, the 3.81 cm ID outer cylinder and the blade that spanned the gap over the 30 cm length. Boundary conditions reflected appropriate no-slip conditions. Velocity profiles were calculated using a segregated solution algorithm for the identical conditions of the MRI mixing

experiments, *e.g.*, same volumetric flow rate, inner cylinder rotation, and fluid properties. The excellent agreement between MRI velocity profiles for this geometry and the finite element analysis have been reported in Wang *et al.* (1999) and are given in detail in Wang (1997).

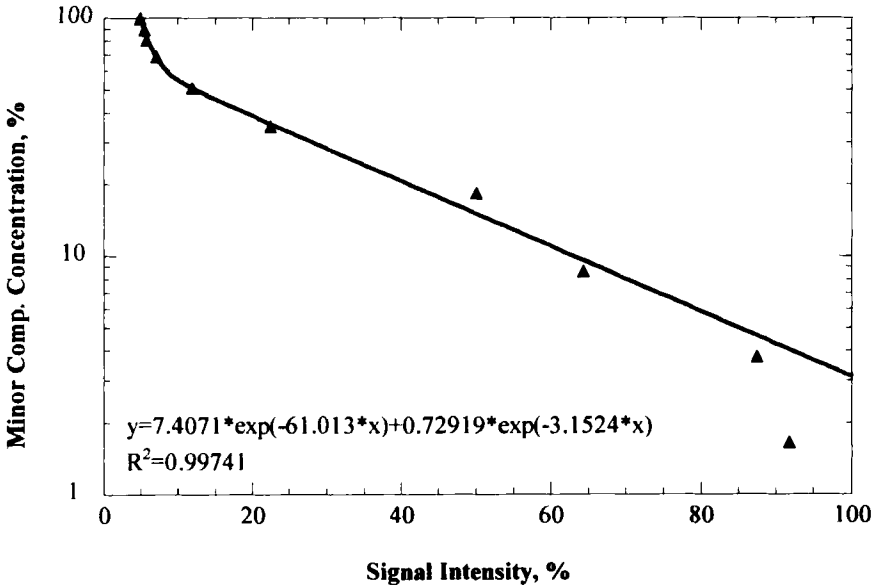

FIG. 2. CALIBRATION CURVE FOR SIGNAL INTENSITY USING MANGANESE CHLORIDE AS AN NMR DOPING COMPOUND

RESULTS AND DISCUSSION

Concentration Images

In this work, concentration images were obtained under four experimental conditions for 1 % carboxymethyl cellulose (CMC) solution. This work focused on the effect of rotation speed and axial flow rate to mix major and minor components that have essentially identical physical properties. These four experimental conditions were characterized by their Reynolds numbers in the axial and angular directions, as defined by:

$$Re_{axial} = \frac{\rho U(D_o - D_i)}{\eta}; \qquad Re_{ang} = \frac{\rho \Omega D_o^2}{\eta}; \tag{2}$$

where ρ is the fluid density, η is the apparent viscosity of the power law fluid, U is the average velocity in the axial direction, Ω is the rotation rate in rad/s, D_i and D_o are the inner and outer cylinder diameter, respectively. The apparent viscosity was evaluated at a characteristic shear rate that includes both axial and angular components evaluated at the wall. Apparent viscosity values varied from 23 to 28 Poise depending on the operating conditions. Both the angular and axial Reynolds numbers fell in the laminar flow regime, at values less than 1.0. However, the relative contribution of angular flow to axial flow, which was characterized by Re_{ang}/Re_{axial}, varied by a factor of four from 32 to 130 (Table 1).

TABLE 1.
REYNOLDS NUMBERS, STATISTICAL PARAMETERS AND WATS FOR 1% CMC SOLUTION AT FOUR OPERATING CONDITIONS

Axial flow rate (ml/min)	*Rotation speed (rpm)*	Re_{ang}	Re_{ang}/Re_{axial}	*I, Intensity*	*Length Scale, (cm)*	*WATS*
45	7.5	0.41	66	0.36	2.24	643
45	15	0.89	130	0.40	1.98	1273
92	7.5	0.48	32	0.68	2.36	302
92	15	0.99	64	0.79	2.29	589

Proton images were obtained for the four experimental conditions at an axial location 20 cm from the introduction of the manganese chloride doped minor component. The signal intensities were converted to percent minor component and are displayed in Fig. 3. These images were analyzed statistically, which provides a quantitative description of the mixing images based on the variance and correlation. The variance, S^2, was calculated by:

$$S^2 = \frac{\sum_{i=1}^{m}(C_i - \bar{C})^2}{m-1} \tag{3}$$

where C_i is the concentration of the minor component from the ith sample (pixel), $\bar{C}$ is the mean concentration of the mixture and m is the total number sample points. The mixing intensity is the normalized variance:

$$I = \frac{S^2}{S_0^2} \tag{4}$$

where S_0^2 is the maximum variance. The second statistic, the mixing length scale, is in terms of a coefficient of correlation $R(r)$:

$$R(r)=\frac{\sum_{i=1}^{N}[C_i(r)-\bar{C}][C_i(r+\Delta r)-\bar{C}]}{NS^2} \tag{5}$$

where $C_i(r)$ and $C_i(r+\Delta r)$ are concentrations at two points at a distance Δr from each other, and N is the total number of randomly paired samples at a distance r. $R(r)$ ranges from 1, where both points have the same concentration, (*e.g.*, a perfect correlation at $r = 0$) to 0, where there is no correlation between the two concentrations (at $r = \beta$). The mixing length scale ς is defined as the integral of the coefficient of correlation $R(r)$ with respect to r from 0 to β:

$$\varsigma=\int_0^{\beta} R(r)dr \tag{6}$$

This value is characteristic of the distance between like components in the cross section.

In each of the images, the minor component is concentrated in the darker regions near the rotating inner cylinder and blade and adjacent to the stationary outer cylinder (Fig. 3). At low axial flow rate, the intensity of mixing is lower (*e.g.*, better mixing) (Table 1). The intensity of mixing also decreased as the angular rotation speed decreased. The combined effect of lower rotation speed and lower axial velocity generated the best mixing, which was characterized by the most uniform signal intensity (at 7.5 rpm, 45 mL/min). A change of axial velocity gave a more pronounced decrease in mixing intensity than a change of rotation speed, which indicates that mixing intensity is governed by residence time in the apparatus, as characterized by Re_{axial}.

The mixing length scale exhibited a different trend than the mixing intensity. The operating condition of 45 mL/min and 15 rpm produced the lowest value of mixing length scale. The length scale was 1.98 cm at a Re_{ang}/Re_{axial} of 130. The operating conditions of 45 mL/min and 7.5 rpm, and 92 mL/min and 15 rpm had similar values of length scale, at approximately the same values of Re_{ang}/Re_{axial} (*i.e.*, ~65). The length scale at an axial velocity of 92 mL/min and 7.5 rpm gave the highest value at 2.36 cm with the lowest Re_{ang}/Re_{axial}. The trend of the length scale with Re_{ang}/Re_{axial} illustrates that mixing is strongly influenced by the relative contribution of angular and axial flow, with high values corresponding to lower length scale values.

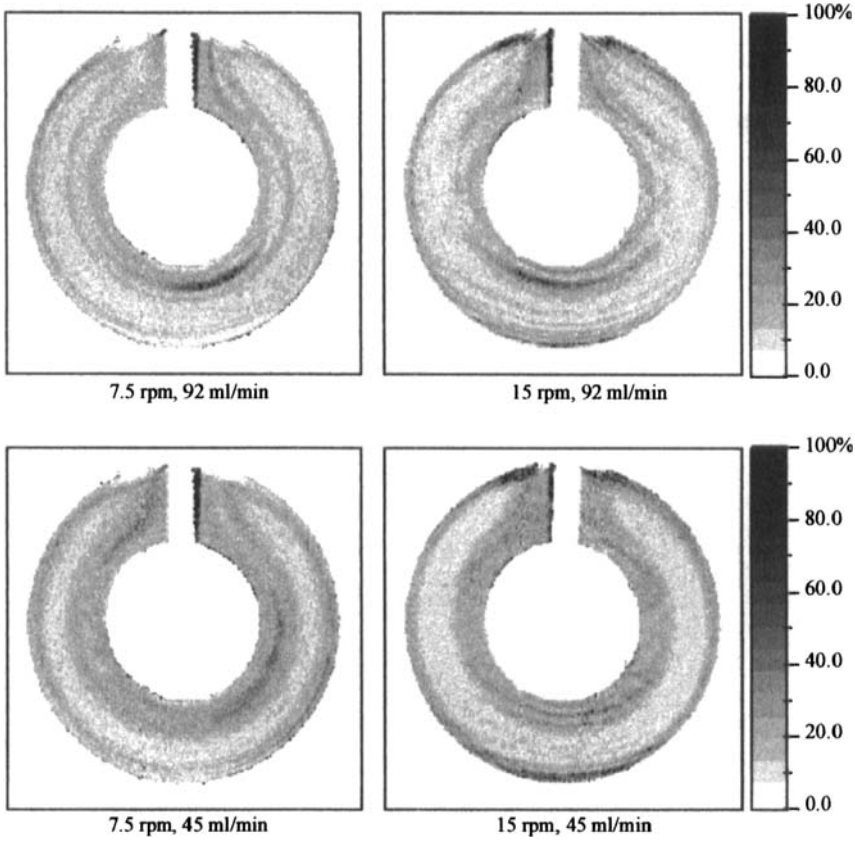

FIG. 3. CONCENTRATION PROFILES AS PERCENT MINOR COMPONENT IN THE SSHE GEOMETRY FOR THE OPERATING CONDITIONS GIVEN IN TABLE 1

Velocity Profiles

To complement the statistical analyses, velocity profiles were obtained to calculate strain and its relationship to mixedness through WATS. Velocity profiles in the angular direction were obtained numerically for the 1% CMC solution. The velocity profiles shown in Fig. 4a illustrate the characteristic drag flow contribution at the rotating inner cylinder and the pressure flow due to the blade. The velocity was normalized by the average angular velocity; position

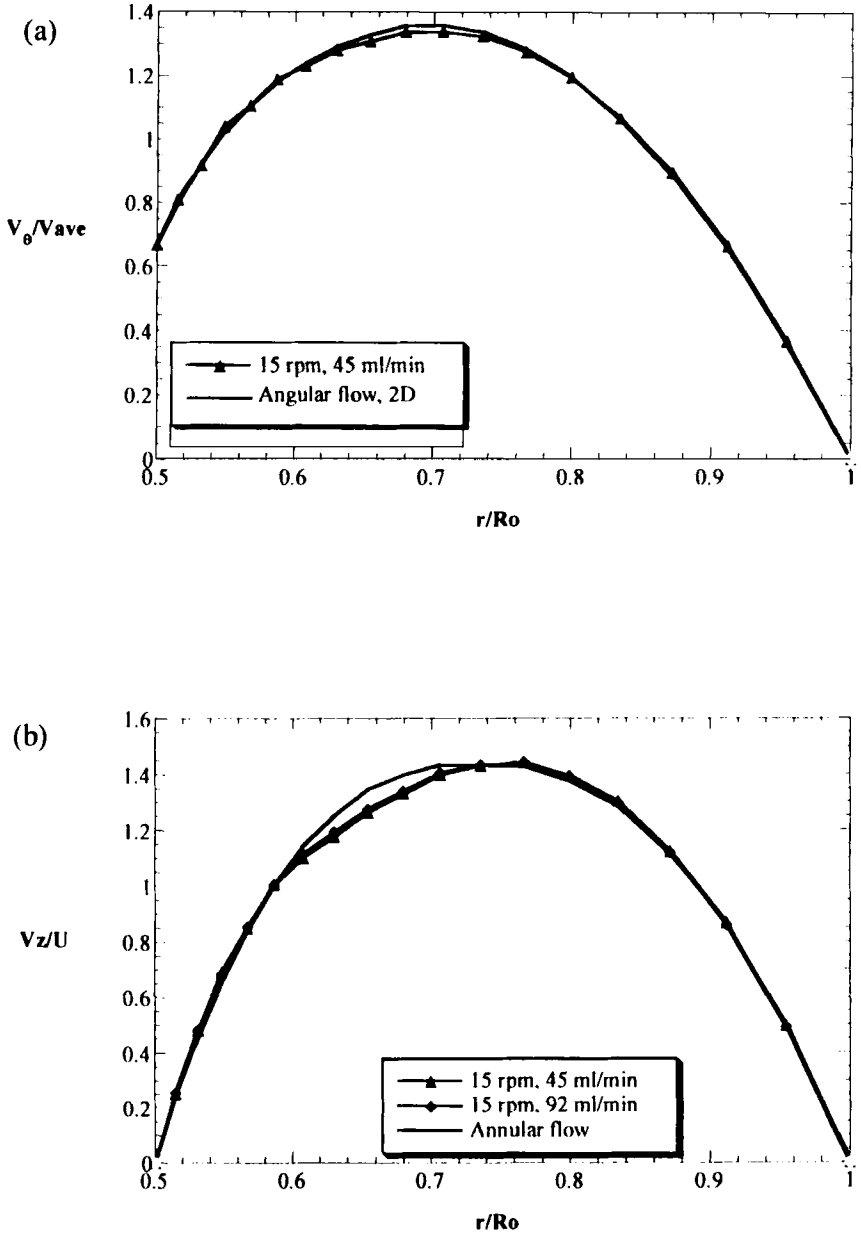

FIG. 4. VELOCITY PROFILES IN THE ANGULAR DIRECTION AND AXIAL DIRECTION FOR THE 1% CMC SOLUTION

was normalized by the outer radius dimension. For comparison, the two-dimensional numerical solution (no axial flow) is shown with the profile from the three-dimensional simulation under the conditions of 15 rpm and 45 mL/min. Although the flow equations are coupled through the shear dependent viscosity, the velocity profile in the angular direction is not significantly affected by flow in the axial direction under these low Reynolds Number conditions. The theoretical velocity profiles for axial flow are shown in Fig. 4b. If the axial and angular flow components were not coupled through the shear dependent viscosity, the axial profile would exhibit the annular flow behavior illustrated as a limiting case. However, the coupling of the flow equations results in asymmetry as seen by a flattening of the profile and shift of the maximum velocity toward the outer cylinder wall, as illustrated for the two flow rates at a inner cylinder/blade rotation of 15 rpm.

The weighted average total strain is based on the shear rate and residence time, both being a function of local velocity. For this cylindrical geometry, the shear rate was evaluated from the velocity gradient in the angular and axial directions,

$$\dot{\gamma} = \left[(\dot{\gamma}_{r\theta})^2 + (\dot{\gamma}_{rz})^2\right]^{1/2} = \left[\left(r\frac{\partial}{\partial r}\left(\frac{v_\theta}{r}\right)\right)^2 + \left(\frac{\partial v_z}{\partial r}\right)^2\right]^{1/2} \tag{7}$$

where v_θ and v_z are velocity components in the angular and axial directions, respectively. The local strain is calculated by the product of the shear rate and residence time at a specified spatial location. The value of WATS is the integral of the total strain weighted by the fraction of the fluid experiencing that strain. For the closed type SSHE geometry, the expression for WATS at a cross sectional position is given in terms of shear rate by (Wang 1997):

$$WATS = \frac{2L}{U(R_0^2 - R_i^2)} \int_{R_i}^{R_0} \dot{\gamma}\, r dr \tag{8}$$

where L is the axial distance that the fluid has traveled, U is the average axial velocity, R_i and R_0 are the inner and outer cylinder radii, respectively.

The total strain and WATS were calculated for the test conditions. Total strain for these operating conditions is illustrated in Fig. 5; high strain regions are near the inner and outer cylinder. The conditions of low axial flow rate, 45 mL/min, and high rotation speed, 15 rpm, gave the highest WATS at 1273. WATS at 45 mL/min and 7.5 rpm was 643, similar to the value at 92 mL/min

and 15 rpm. The lowest WATS was 302 at 92 mL/min and 7.5 rpm. Similar to the mixing length scale, the WATS was affected by the ratio of Reynolds numbers; higher values of Re_{ang}/Re_{axial} resulted in higher values of WATS and lower values of length scale. In other words, improved mixing is characterized by decreasing scale of segregation.

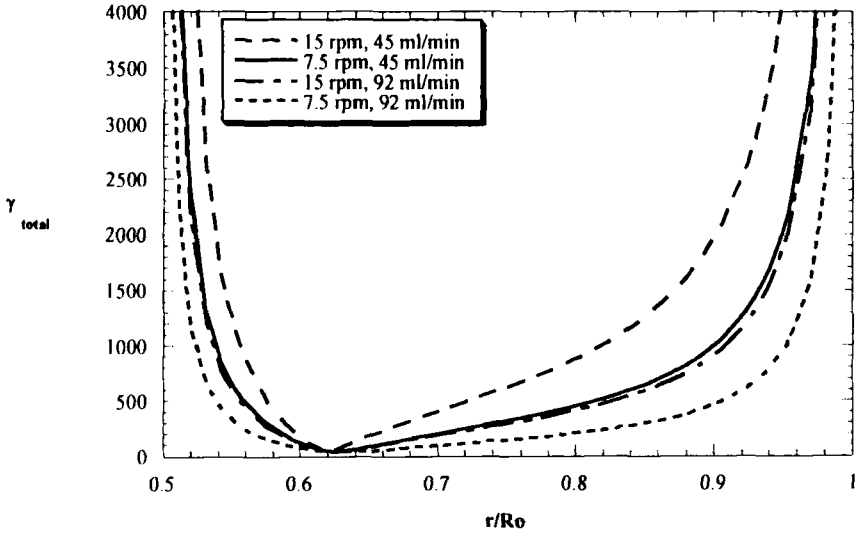

FIG. 5. TOTAL STRAIN AS A FUNCTION OF POSITION FOR 1% CMC SOLUTION UNDER THE FOUR OPERATING CONDITIONS GIVEN IN TABLE 1

Figure 6 displays the total strain contour of the cross section at an axial location of L=15 cm. The dark region represents the high strain area (better mixing) and the light region illustrates the low strain area (poorer mixing). The better mixing regions are located near the blade and near the inner and the outer cylinders. The low strain area, the narrow bright band in the annulus, is the least mixed region. This contour plot of the total strain obtained from the numerical simulation exhibits excellent agreement with the concentration images obtained by MRI (Fig. 3).

This work demonstrates the relationship between the strain analysis and the statistical mixing analysis in terms of comparing the strain map with the associated concentration profile. Future studies will focus on evaluating increasing values of $Re_{angular}/Re_{axial}$ in order to better simulate mixing in commercial scraped surface heat exchange geometries.

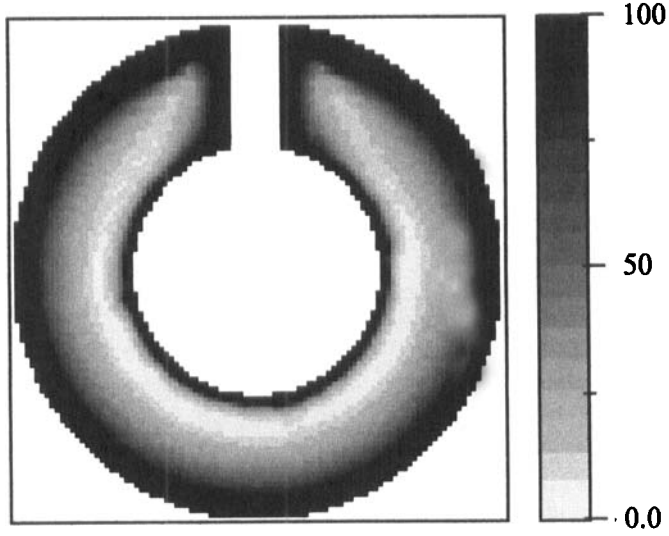

FIG. 6. CONTOUR OF TOTAL STRAIN FOR 1% CMC SOLUTION AT 15 RPM, 45 ML/MIN

NOMENCLATURE

C_i	concentration of the minor component from the ith sample (pixel)
$\bar{C}$	mean concentration of the mixture
D_i	inner cylinder diameter
D_o	outer cylinder diameter
I	mixing intensity
K	power law consistency index
L	axial distance
m	total number samples
m	constant related to the sample and its chemical and physical environment
n	power law flow behavior index
N	total number of randomly paired samples
r	radial dimension
$R(r)$	coefficient of correlation
R_i	inner radius
R_0	outer radius
Re	Reynolds Number
S^2	variance
SI	signal intensity
T_1	spin-lattice relaxation time

T_2 spin-spin relaxation time
TE echo time
TR repetition time
U average axial velocity
v_θ velocity component in the angular direction
v_z velocity component in the axial direction
$WATS$ weighted average total strain
z axial direction

Greek symbols

β radial dimension denoting zero correlation
γ strain
$\dot{\gamma}$ shear rate
η apparent viscosity, calculated with wall shear rates in the axial and annular directions
θ angular direction
ρ fluid density
Ω rotation rate
ς mixing length scale

REFERENCES

ALCAIRO, E.R. and ZURITZ, C.A. 1990. Residence time distributions of spherical particles suspended in non-Newtonian flow in a scraped-surface heat exchanger. Trans. ASAE *33*, 1621–1628.

BIGG, D. and MIDDLEMAN, S. 1974. Mixing in a screw extruder. A model for residence time distribution and strain. Ind. Eng. Chem. Fundamental *13*, 66–71.

BOOY, M.L. 1963. Influence of channel curvature on flow, pressure distribution, and power requirements of screw pumps and melt extruders. Soc. Plastics Engineers Trans. *3*, 176–185.

BOTT, T.R., AZPPRU, S. and PORTER, K.E. 1968. Scraped-surface heat exchangers. Part II - The effects of axial dispersion on heat transfer. Trans. Institution Chem. Eng. *46*, T37–43.

CORBETT, A.M., PHILLIPS, R.J., KAUTEN, R.J. and MCCARTHY, K.L. 1995. Magnetic resonance imaging of concentration and velocity profiles of pure fluids and solid suspensions in rotating geometries. J. Rheology *39*, 907–924.

DYAKOWSKI, T. 1996. Process tomography applied to multi-phase flow measurement. Measurement Sci. Technol. *7*, 343–353.

GRIFFITH, R.M. 1962. Fully developed flow in screw extruders, theoretical and experimental study. Ind. Eng. Chem. Fundamental *1*, 180–187.

HARPER, J.M. 1981. *Extrusion of Foods*, Vol. 1, pp. 93–106, CRC Press, Boca Raton, Florida.

KOOL, J. 1958. Heat transfer in scraped vessels and pipes handling viscous materials. Trans. Institution Chemical Eng. *36*, 253–258.

MCCARTHY, M.J. 1994. *Magnetic Resonance Imaging in Foods*, Chapman & Hall, New York.

MCKELVEY, J.M. 1962. *Polymer Processing*, John Wiley & Sons, New York.

MIDDLEMAN, S. 1977. *Fundamentals of Polymer Processing*, pp. 295–348, McGraw-Hill Book Co., New York.

PINTO, G. and TADMOR, Z. 1970. Mixing and residence time distribution in melt screw extruders. Polymer Eng. Sci. *10*, 279–288.

RAMASWAMY, H.S., ABDELRAHIM, K.A., MARCOTTE, M. and CLAVIER, P. 1995. Residence time distribution (RTD) characteristics of meat and carrot cubes in starch solutions in a vertical scraped surface heat exchanger (SSHE). Food Res. Intl. *28*, 331–342.

ROMBACH, K., LAUKEMPER-OSTENDORF, S. and BLUMLER, P. 1998. Applications of NMR flow imaging in material science. In *Spatially Resolved Magnetic Resonance: Methods and Applications in Material Science, Agriculture and Biomedicine*, (B. Blumich, P. Blumler, R. Botto, and E. Fukushima, eds.) Aachen, Germany.

SMITH, E.G., KOHLI, R., MARTINE, P.A., ROBERTS, N. and EDWARDS, R.H.T. 1995. MRI for assessing mixing quality. In *Frontiers in Industrial Process Tomography*, (D.M. Scott and R.A. Williams, eds.) Engineering Foundation, New York.

TADMOR, Z. and GOGOS, C.G. 1979. *Principles of Polymer Processing*, pp. 196–240, 404–466, John Wiley & Sons, New York.

TROMMELEN, A.M. and BEEK, W.J. 1971. Flow phenomena in a scraped-surface heat exchanger ("Votator"-type). Chem. Eng. Sci. *26*, 1933–1942.

WANG, W. 1997. Experimental aspects of mixing in scraped surface heat exchanger geometry. Ph.D. Dissertation, Dept. Biological and Agricultural Engineering, University of California, Davis.

WANG, W., WALTON, J.H. and MCCARTHY, K.L. 1999. Flow profiles of power law fluids in scraped surface heat exchanger geometry using MRI. J. Food Process Engineering *22*, 11–27.

WANG, W., WALTON, J.H., MCCARTHY, M.J. and MCCARTHY, K.L. 1998. Evaluation of mixing profiles of power law fluids in scraped surface heat exchanger geometry using MRI. In *Spatially Resolved Magnetic Resonance: Methods and Applications in Material Science, Agriculture and Biomedicine*, (B. Blumich, P. Blumler, R. Botto and E. Fukushima, eds.) Aachen, Germany.